



GREEN SYNTHESIS, STRUCTURAL AND OPTICAL PROPERTIES OF CLERODENDRUM INFORTUNATUM MEDIATED-SILVER DOPED COBALT OXIDE NANOPARTICLES: ASSESSMENT OF ITS ANTICANCER ACTIVITY

Harikumar Renuka UMA^{a,c} and Jessica FERNANDO^{b,c,*}

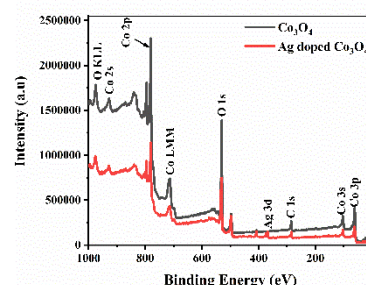
^a Research Scholar (Register No: 20113112032013) Department of Chemistry, V. O. Chidambaram College, Thoothukudi, Tamil Nadu, India-628008

^b Associate Professor, Department of Chemistry, V. O. Chidambaram College, Thoothukudi, Tamil Nadu, India-628008

^c Affiliated to Manonmaniam Sundaranar University, Abishekapatti, Tamil Nadu, India – 627012

Received March 22, 2025

Transition metals have been widely explored as potential optical dopants, offering a promising route for achieving innovative materials. In recent years, metal oxides synthesized using *Clerodendrum infortunatum* leaf extract have emerged as novel anticancer agents. This study reports the sustainable synthesis of Ag-doped Co_3O_4 nanoparticles using *Clerodendrum infortunatum* aqueous extract as a bio-reductant. The resulting pure Co_3O_4 and Ag-doped Co_3O_4 nanoparticles were characterized using XRD, EDS, XPS, UV-Vis, and PL spectroscopy. The PL spectra revealed that Ag-doped Co_3O_4 nanoparticles exhibited more intense defect emissions compared to the pristine samples. Furthermore, MTT assays using AGS (Human Gastric Adenocarcinoma) cells demonstrated the enhanced anticancer activity of the doped nanoparticles over their bare counterparts. These findings suggest that Ag-doped Co_3O_4 nanoparticles hold promise as a viable alternative for anticancer materials, particularly in biomedical applications.



INTRODUCTION

The use of plant extracts has gained significant attention as a sustainable approach for nanoparticle synthesis. Plant extracts are readily available, considered safe to handle, and offer a diverse range of metabolites.¹ As a renewable and abundant resource, plants provide low-cost, non-toxic, and biocompatible phytomaterials with varied chemical properties.² As a result, there is a growing emphasis

on utilizing plant extracts to develop eco-friendly methods for producing pure, biocompatible, and non-toxic nanoparticles.^{3,4} In recent years, the biosynthesis of nanoparticles using biological matrices has emerged as a viable alternative to chemical and physical preparation methods. This approach is easy to implement, safe, cost-effective, and environmentally acceptable.^{5–7} Cobalt oxide nanoparticles have garnered significant interest among researchers due to their unique

* Corresponding author: drjessicafernando@gmail.com

physicochemical properties, which distinguish them from their bulk counterparts. Cobalt oxide nanoparticles have been widely utilized in various industries, including biomedical,⁸ photocatalysis,⁸ gas sensing,⁹ and solar cells.¹⁰ Research has shown that doping Co_3O_4 with transition metals like Ag, Ce, Ni, F, and Cd can enhance its properties.^{11–17} Among these dopants, Ag has garnered significant attention due to its high energy and potential biomedical applications.¹¹ For instance, Alema *et al.*¹⁸ synthesized Ag-doped Co_3O_4 nanoparticles using co-precipitation for high-performance supercapacitors. Ag-doped Co_3O_4 nanostructures have been found to exhibit promising applications in photocatalysis,^[19] non-enzymatic glucose sensing,²⁰ supercapacitors,¹⁸ gas sensing,²¹ and other areas. Various methods have been employed to prepare metal-doped Co_3O_4 nanoparticles.^{16–21}

However, biosynthesis has emerged as a viable, eco-friendly, and cost-effective alternative to traditional chemical and physical processes. Plant-mediated synthesis, also known as green chemistry, offers a promising approach to integrating nanotechnology and plant-based methods.²² The eco-friendly method of green synthesis offers a promising approach for creating nanostructures, with potential applications in biomedicine, agriculture, and environmental remediation.²³

This method leverages the secondary metabolites present in various plant parts (such as peels, leaves, flowers, roots, seeds, and stems) to synthesize nanostructures.²⁴ Specifically, the secondary metabolites in leaf extracts serve as reducing and stabilizing agents, facilitating the transformation of metal ions into metal oxide nanoparticles. Vindhya *et al.*²⁵ reported that the plant extract contains various phytochemicals such as polyphenols, flavonoids, and secondary metabolites, which act as potential candidates for reducing, stabilizing, and capping agents toward the formation of nanoparticles and for biological applications.

They also noted that careful control and documentation of capping agents and appropriate functional groups on the nanoparticle surface enable regulation of particle size, shape, agglomeration, surface energy, grain development, dispersion, and electrostatic forces. Previous study by Kumar *et al.*²⁶ demonstrated the phyto-mediated synthesis of zinc oxide nanoparticles using Clerodendrum infortunatum L. leaf extract, which exhibited

enhanced antibacterial properties. To our knowledge, this study presents the first report on the use of Clerodendrum infortunatum L. leaf extract for doping elements into Co_3O_4 nanoparticles. Here, we report the green synthesis of undoped Co_3O_4 and Ag-doped Co_3O_4 nanoparticles using Clerodendrum infortunatum leaf extract, characterized by XRD, TEM, EDS, XPS, UV–visible, and PL spectroscopy. The anticancer potential of these nanoparticles was evaluated using MTT assays.

MATERIALS AND METHODS

Materials

The chemical reagents employed in this study were cobalt nitrate and silver nitrate (AgNO_3), both of which were procured from SRL Chemicals with a guaranteed purity of 99%. All reagents used were of analytical grade and were utilized without additional purification. Double-distilled (DD) water was used as the solvent for preparing all aqueous solutions.

Preparation of leaf Extract

Clerodendrum infortunatum leaves were collected, cleaned with tap water, and then repeatedly rinsed with DD water to remove impurities. The leaves were then dried and subsequently boiled in 150 mL of DD water at 80°C, using 30 g of leaves. This process yielded a yellow-colored extract. After reaching room temperature, the extracted mixture was filtered using Whatman filter paper and stored in the refrigerator for future use.

Synthesis of pure cobalt oxide nanoparticles

A solution was prepared by dissolving 5 g of cobalt nitrate in 50 ml of double-distilled water. Then, 10 ml of Clerodendrum infortunatum leaf extract were added to the solution under continuous stirring. The pH of the mixture was adjusted to 7 by adding sodium hydroxide. The solution was then stirred magnetically for 2 hours, resulting in the formation of a precipitate. The solution was left undisturbed for 24 hours to allow the precipitate to settle. The precipitate was subsequently filtered, washed with double-distilled water and ethanol, and dried. Finally, the obtained powder was calcined at

500 °C for 2 h in a muffle furnace to prepare it for subsequent characterization.

Synthesis of silver doped cobalt oxide nanoparticles

Aqueous solutions of cobalt nitrate (5g) and silver nitrate (0.5 g) were prepared using 50 ml of double-distilled water. The solutions were then combined and stirred continuously as 10ml of leaf extract were added. The pH of the mixture was adjusted to 7 using sodium hydroxide. After two hours of magnetic stirring, the solution was left to settle for 24 hours, resulting in the formation of a precipitate. The precipitate was subsequently filtered, washed with double-distilled water and ethanol, dried. Finally, the obtained powder was calcined at 500 °C for 2 h in a muffle furnace to prepare it for subsequent characterization.

Characterization techniques

The crystal structure, phase composition, and average crystallite size of the synthesized samples were characterized using X-ray diffraction (XRD) on a PANalytical X'Pert Pro diffractometer, equipped with Cu-K α radiation ($\lambda = 1.5406 \text{ \AA}$) and operated at 40 kV and 30 mA. Transmission electron microscopy (TEM) was performed on a JEOL JEM-2100F microscope, operating at 200 kV, to obtain nanoparticle micrographs. Energy Dispersive X-ray Spectroscopy (EDS) was carried out on Bruker Nano GmbH Berlin, Germany (Esprit 1.9). X-ray photoelectron spectroscopy (XPS) analysis was carried out on a PHI 5000 Versa Probe 111 spectrometer, equipped with a high-performance Ar⁺ ion gun and C60 ion guns, to investigate the Co 2p, O 1s, and Ag 3d peaks. The optical properties of the samples were evaluated by UV-Vis spectroscopy using a Perkin Elmer LAMBDA-35 spectrophotometer at room temperature. Photoluminescence (PL) spectra were recorded on a Cary Eclipse Photoluminescence Spectrophotometer at room temperature.

Anticancer activity

The human stomach adenocarcinoma cell line AGS was procured from the National Centre for Cell Science (NCCS) in Pune, India. The cells were sub-cultured in DMEM/F12 medium supplemented with 10% fetal bovine serum (FBS) and 1%

antibiotic-antimycotic solution in a humidified atmosphere of 5% CO₂, 18-20% O₂, and 37 °C temperature. The cells were passaged 37 times before use. For the experiment, 200 μ l of cell suspension was seeded at a density of 10,000 cells per well in a 96-well plate and allowed to grow for 24 hours. Test chemicals were then added at specified concentrations, and the plate was incubated for an additional 24 hours at 37°C with 5% CO₂. After incubation, the media was discarded, and MTT reagent was added to a final concentration of 0.5 mg/ml. The plate was then incubated for 3 hours in the dark. Following MTT removal, 100 μ l of DMSO solubilization solution was added, and the plate was gently shaken to dissolve the formazan crystals. Absorbance was measured at 570 nm using a spectrophotometer or ELISA reader. The following formula was used to get the proportion of viable cells.

$$\text{Cell Viability (\%)} = \frac{\text{OD sample mean}}{\text{OD control mean}} \times 100 \%$$

RESULTS AND DISCUSSION

XRD analysis

The XRD patterns of as-synthesized Co₃O₄ and Ag doped Co₃O₄ nanoparticles are shown in Fig. 1. The peaks at $2\theta = 31.53, 37.22, 45.03, 56.28, 59.58$ and 65.55° correspond to the planes (220), (311), (400), (422), (511) and (440), respectively, confirming a FCC cubic crystal system (JCPDS file no: 42-1467).^{27,28} The average crystallite size was calculated using Debye Scherrer formula (eq. 1):

$$D = \frac{0.9\lambda}{\beta \cos \theta} \quad (1)$$

The variables 'D', ' θ ', and ' β ' represent the average crystalline size, diffraction angle, and full width at half maximum (FWHM) of the diffraction peak under investigation in radians, respectively, while the wavelength of Cu K α radiation is $\lambda = 1.5405 \text{ \AA}$. The calculated mean crystallite sizes for the pure Co₃O₄ and Ag doped Co₃O₄ nanoparticles are 24.3 and 19.6 nm respectively. The reduced crystallite size observed in the doped sample indicates that the incorporation of Ag ions hinders both the nucleation and growth processes of the Co₃O₄ structure.²⁹

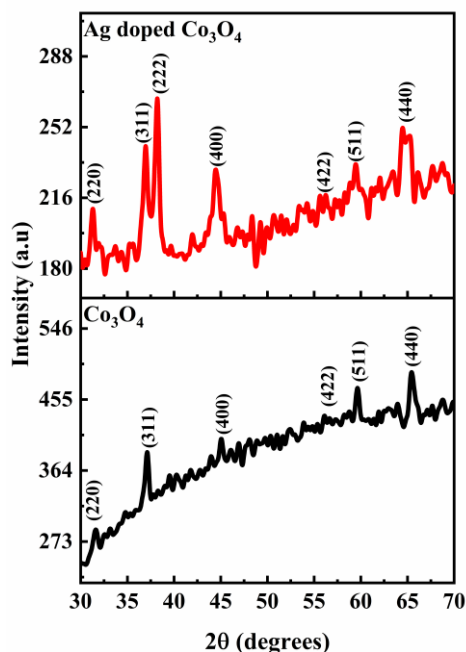


Fig. 1 – XRD spectra of pure Co_3O_4 and Ag doped Co_3O_4 nanoparticles.

TEM analysis

The morphology of the typically synthesized Ag doped Co_3O_4 nanoparticles was investigated by TEM and HRTEM, as shown in Fig. 2. Clearly, the as-obtained sample (Fig. 2a) consists of closely packed spherical shaped structures with the diameter of around twenty nanometers. Figure 2b shows the HRTEM image of the Ag doped Co_3O_4

nanoparticles. The lattice fringe can be observed clearly, and the inter plane distances of adjacent lattice fringes is about 0.26 nm (2.6 \AA), which is in good agreement with the d value of (311) plane of Co_3O_4 nanoparticles. Based on the above analysis, it confirms that spherical shaped structures and well crystalline nature of Ag doped Co_3O_4 nanoparticles could be synthesized by the Clerodendrum infortunatum L. leaf extract.

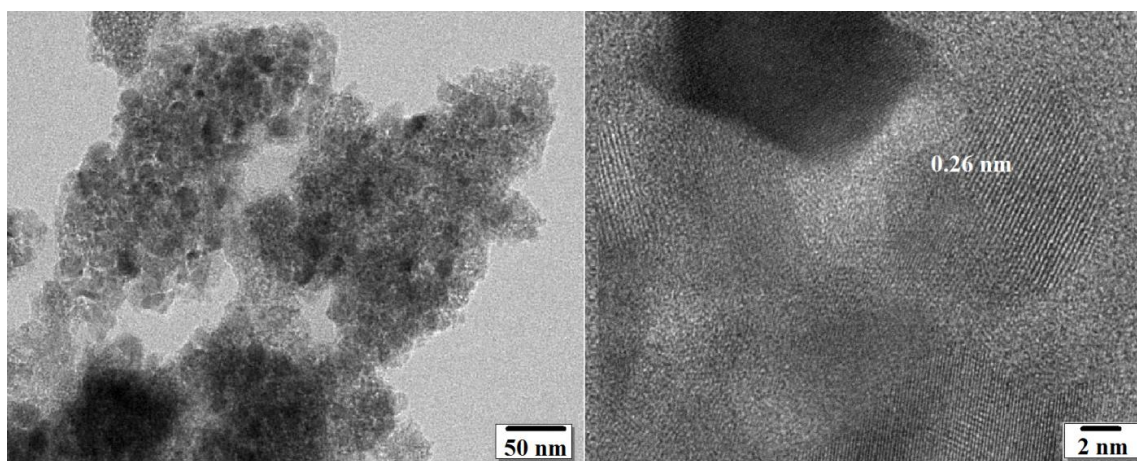


Fig. 2 – Micrograph of: a) TEM; b) HRTEM of Ag doped Co_3O_4 nanoparticles.

EDS spectral analysis

Figure 3a presents the EDS spectrum of the pure Co_3O_4 sample. It exhibits distinct peaks for cobalt

(Co) and oxygen (O), confirming the phase purity of the material. Quantitative analysis (inset table) reveals a composition of 52.81 wt% Co and 47.19 wt% O, equivalent to 67.25 at% Co and

32.75 at % O. The EDS spectrum of the Ag-doped Co_3O_4 (Fig.3b) displays an additional peak corresponding to silver (Ag), indicating successful incorporation of Ag into the Co_3O_4 lattice. The

measured elemental composition (inset) is 44.83 wt % Co, 42.25 wt % O, and 12.92 wt % Ag, which translates to atomic percentages of 47.93 % Co, 49.84 % O, and 2.23 % Ag.

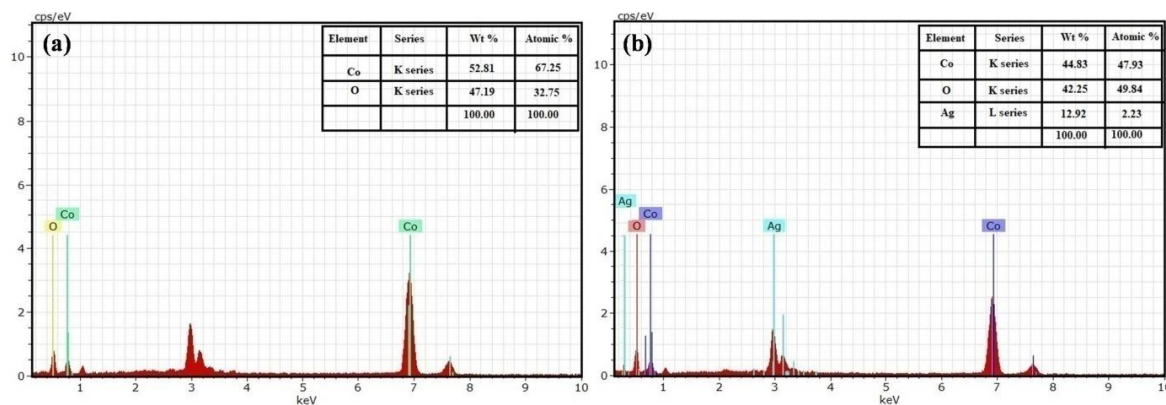


Fig. 3 – EDS spectra of: a) pure Co_3O_4 ; b) Ag doped Co_3O_4 nanoparticles.

XPS spectra

XPS analysis was conducted to determine the chemical states and elemental composition of the as-synthesized materials. The survey spectra (Fig. 4) revealed the presence of Co, O and Ag as primary elements in the sample. The Co_3O_4 spectrum displayed characteristic auger peaks and emission lines for Co and O, while the Ag doped Co_3O_4 survey spectrum further showed the emission line of Ag, confirming successful doping. The detected core levels included Co 2s, Co 2p, Co 3s, Co 3p, O 1s and Ag 3d, along with auger peaks Co LMM and O KLL. The appearance of C 1s is attributed to adventitious carbon, resulting from air exposure. Co_3O_4 is a mixed-valence oxide

containing Co^{2+} and Co^{3+} . In XPS, the Co 2p region shows two main peaks (≈ 780 eV and ≈ 795 eV) and their satellite structures. Co^{2+} gives a strong shake-up satellite about 5–6 eV higher than the main $2p_{3/2}$ peak. Co^{3+} has a very weak satellite and its photoelectrons often overlap with the Co^{2+} main peak, making the Co^{3+} component hard to resolve. Therefore, even though Co^{3+} is present in the material, the XPS spectrum may appear dominated by Co^{2+} features, and the Co^{3+} signal can be obscured or not clearly distinguishable.³⁰ The Co 2p spectrum (Fig. 5a) exhibits characteristic Co $2p_{3/2}$ and Co $2p_{1/2}$ spin-orbit peaks at 779.75 eV and 794.76 eV, respectively, along with a satellite peak at 788.75 eV. These XPS profiles indicate the presence of Co in a high-spin divalent state.³¹

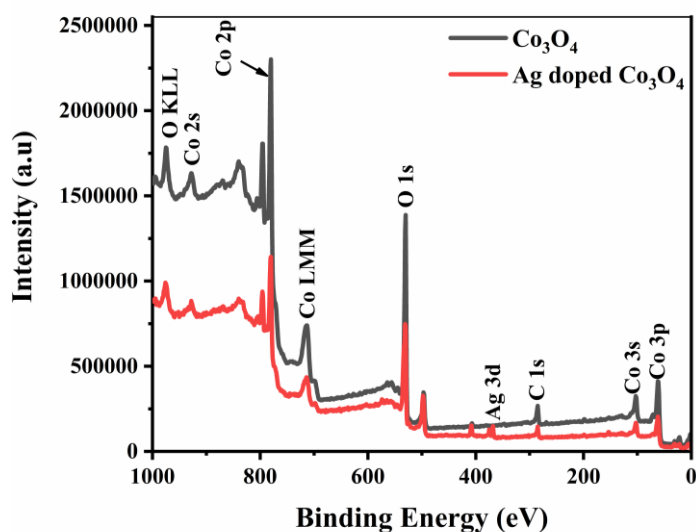


Fig. 4 – X-ray photoemission survey spectra of pure Co_3O_4 and Ag doped Co_3O_4 nanoparticles.

The O 1s spectrum (Fig. 5) was deconvoluted into three peaks, revealing insights into the oxygen species present on the surface of Ag-doped Co_3O_4 . The peak at 532.02 eV is attributed to oxygen vacancies, while the peak at 529.58 eV corresponds to lattice oxygen, confirming the presence of Co_3O_4 . The peak at 530.57 eV is associated with oxygen vacancies that give rise to O^- and O^{2-} ions in the oxygen-deficient region.³² Variations in peak intensity may be due to changes

in the concentration and quantity of oxygen vacancies.³³ The Ag 3d XPS spectrum (Fig. 5c) exhibits two distinct peaks at 368.18 eV ($\text{Ag } 3d_{5/2}$) and 374.26 eV ($\text{Ag } 3d_{3/2}$), corresponding to metallic silver (Ag^0) and silver ions (Ag^+), respectively. These findings are consistent with previous reports.³⁴ The XPS data validate the successful fabrication of pure Co_3O_4 and Ag-doped Co_3O_4 nanoparticles, which was previously confirmed by EDS and XRD studies.

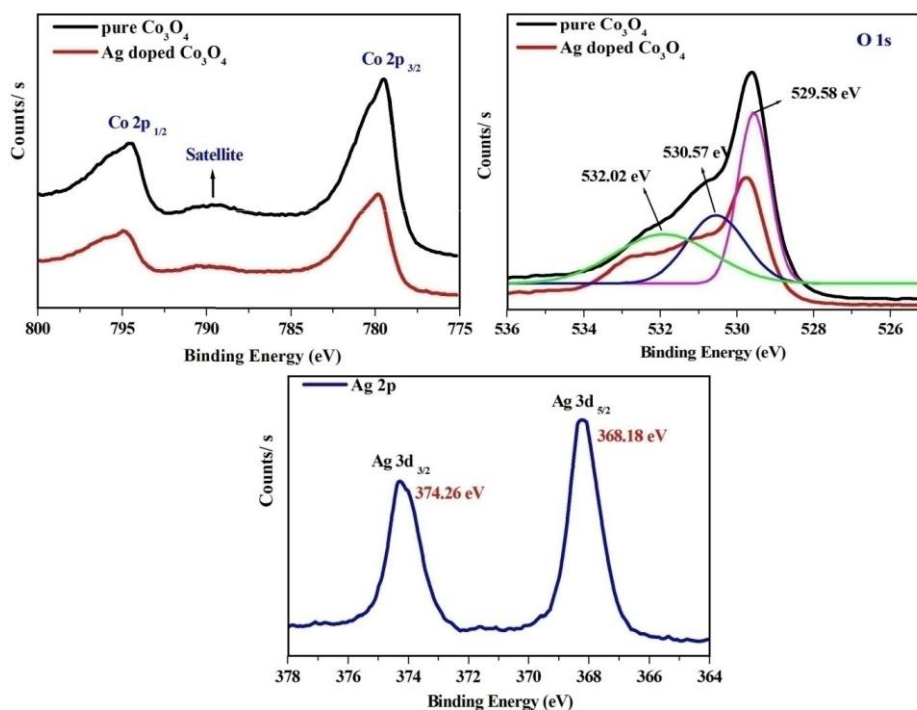


Fig. 5 – XPS spectrum of: a) Co 2p; b) O 1s; c) Ag 3d.

UV-vis spectroscopy

The UV-vis absorption spectra (Fig. 6 (a)) of Co_3O_4 and Ag doped Co_3O_4 nanoparticles

showed a noticeable red shift in the absorption peak upon doping, with centered at 290 nm for Co_3O_4 and 296 nm for Ag doped Co_3O_4 nanoparticles.

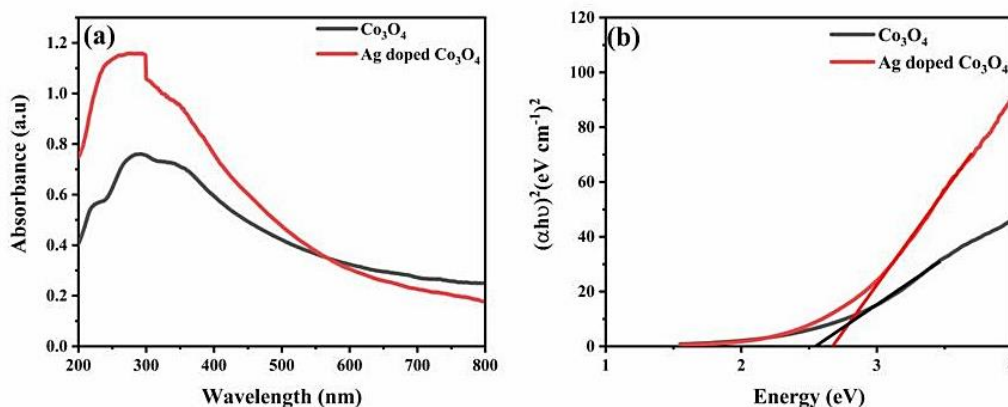


Fig. 6 – a) UV absorbance spectra of Co_3O_4 and Ag doped Co_3O_4 nanoparticles; b) Tauc plot of Co_3O_4 and Ag doped Co_3O_4 nanoparticles

This significant shift indicates a change in the optical absorption behavior due to doping. The band gap energies were calculated using the Tauc plot method based on eq. (2).

$$\alpha h\nu = A(h\nu - E_g)^n \quad (2)$$

where E_g is the band gap energy, $n = 1/2$ is assigned for direct band gap semiconductors, h stands for Planck's constant, A is a constant, and α is the absorption coefficient. In accordance with computations, the Co_3O_4 and Ag doped Co_3O_4 nanoparticles exhibited

band gap energies of 2.54 and 2.68 eV, respectively as reflected in Fig. 6b.

PL spectra

The photoluminescence (PL) spectra of pure and Ag-doped Co_3O_4 nanoparticles, measured at room temperature, are depicted in Fig. 7. The near-band-edge (NBE) emission, corresponding to the UV region (below 400 nm), and the deep-level (DL) emissions, corresponding to the visible region (above 400 nm), are both observed within the UV-Vis luminescence bands.

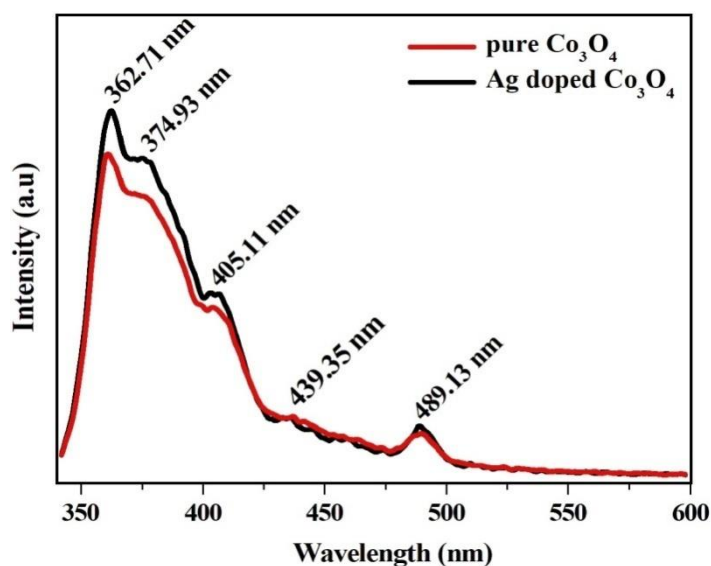


Fig. 7 – PL spectra of pure Co_3O_4 and Ag doped Co_3O_4 nanoparticles.

The addition of Ag dopant resulted in a decrease in emission intensity compared to pure Co_3O_4 nanoparticles, which may be attributed to defects such as single ionized oxygen vacancies.³⁵ In contrast, the emission intensity of Ag-doped Co_3O_4 nanoparticles increased due to enhanced electron-hole recombination in the valence band. The photoluminescence spectra of both samples exhibit three emission peaks in the visible range and a broad UV emission band between 300-400 nm. The NBE emission, corresponding to free excitons in the conduction band, is responsible for the two peaks in the strong UV emission band, occurring at approximately 362.71 nm and 374.93 nm.³⁶ The violet emission peak at 405.11 nm is attributed to interstitial cobalt. The radiative recombination between the deep acceptor (V_o) and shallow donor (Co_i) levels is believed to be responsible for the measured violet emission at 439.35 nm.³⁷ The blue emission peak at 489.13 nm, observed in both

samples, is associated with defect-related emission or surface impurities, such as intrinsic defects, oxygen vacancies, surface states, and interstitial metal ions in the oxide³⁸

Anticancer activity

The MTT assay was employed to evaluate the anticancer potential of green-synthesized pure Co_3O_4 and Ag-doped Co_3O_4 nanoparticles against AGS (Human Gastric Adenocarcinoma) cell lines. The nanoparticles were tested at varying concentrations (6.25–100 $\mu\text{g}/\text{ml}$) to assess their impact on cell viability. The results, presented in Fig. 8, demonstrate that the synthesized nanoparticles significantly reduce the viability of AGS cells. Notably, the highest concentration of 100 $\mu\text{g}/\text{ml}$ exhibited the most pronounced inhibitory effect on AGS cells, outperforming the untreated control.

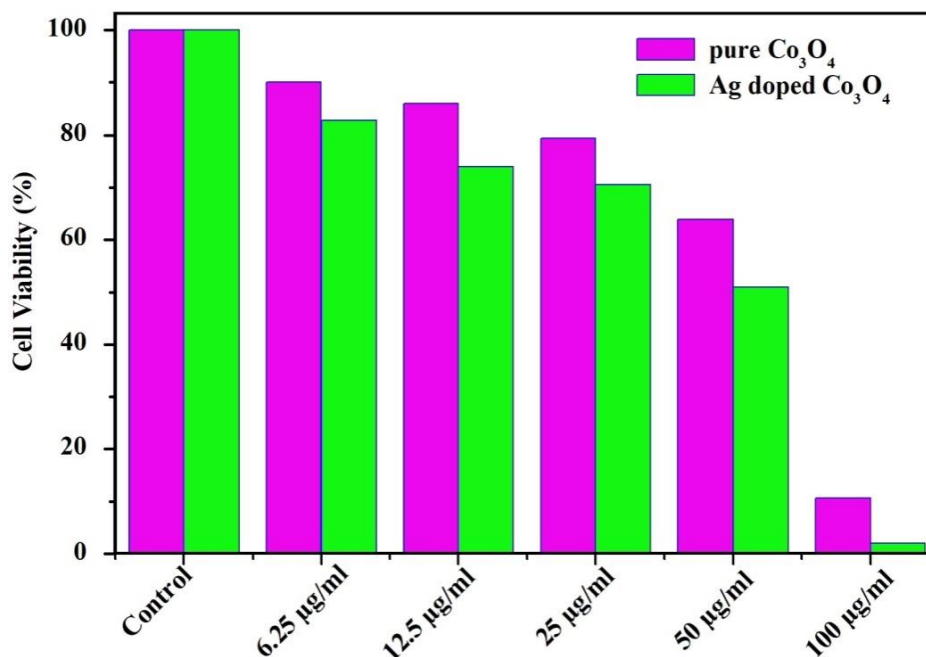


Fig. 8 – % cell viability values of AGS cells treated by different concentrations/ doses of pure Co_3O_4 and Ag doped Co_3O_4 nanoparticles after the incubation period of 24hrs by MTT assay.

The results revealed a concentration-dependent decrease in cell viability for both pure Co_3O_4 and Ag-doped Co_3O_4 nanoparticles. Specifically, the cell viability decreased from 90.10% to 11.66% as the concentration of pure Co_3O_4 increased from 6.25 $\mu\text{g/ml}$ to 100 $\mu\text{g/ml}$. In contrast, the cell viability decreased more significantly from 82.90% to 2.01% as the concentration of Ag-doped Co_3O_4 nanoparticles increased from 6.25 $\mu\text{g/ml}$ to 100 $\mu\text{g/ml}$. These findings suggest that Ag-doped Co_3O_4 nanoparticles exhibit enhanced anticancer activity compared to pure Co_3O_4 nanoparticles, as evidenced by the more pronounced reduction in cell viability.

The cytotoxicity of Co_3O_4 nanoparticles is often attributed to factors such as metal ion release, reactive oxygen species (ROS) production, and particle size.³⁹ Previous studies have shown that Co_3O_4 nanoparticles can induce oxidative stress, genotoxic effects, cell death, DNA damage, and inflammatory responses.⁴⁰ The present study found that Ag-doped Co_3O_4 nanoparticles triggered intracellular ROS production in a dose-dependent manner. Furthermore, the results demonstrated a concentration-dependent decrease in cell survival of AGS cell lines treated with Ag-doped Co_3O_4 nanoparticles, highlighting their potential cytotoxic effects.

The Ag-doped Co_3O_4 nanoparticles disrupt cancer cell function and cause cellular disturbance. Cobalt ions have been shown to be effective against

cancer cells, as they can penetrate cells and generate ROS, leading to apoptosis.⁴¹ Silver ions also induce apoptosis in cancer cells by increasing the levels of free radicals.⁴² These findings suggest that Ag-doped Co_3O_4 nanoparticles may exhibit enhanced anti-tumor cell activity. According to Akhtar *et al.*,⁴³ the increased band gap of metal-oxide nanoparticles contributes to ROS mediated toxicity. The broad band gap of Ag-doped Co_3O_4 nanoparticles plays a crucial role in ROS mediated cytotoxicity. Furthermore, our results indicate that Clerodendrum infortunatum leaf extract-mediated Ag-doped nanoparticles exhibit a stronger cytotoxic effect than their pure counterparts, with the doped silver ion enhancing the rate of induced cytotoxicity.

Figure 9 presents the results of the MTT assay for human AGS cells treated with pure Co_3O_4 and Ag-doped Co_3O_4 nanoparticles. The figure illustrates the dose-dependent suppression of AGS cell growth by the nanoparticles, as evidenced by MTT labeling. The cell survival rates decreased progressively with increasing concentrations of 6.25 $\mu\text{g/ml}$, 12.5 $\mu\text{g/ml}$, 25 $\mu\text{g/ml}$, 50 $\mu\text{g/ml}$, and 100 $\mu\text{g/ml}$. The image reveals significant cell death following treatment with the prepared samples.⁴⁴

When evaluating the potential of nanoparticles for biomedical applications, particularly in vivo, toxicity is a crucial consideration. Nanoparticles designed for imaging and drug delivery are often intentionally coated with bioconjugates such as proteins, DNA,

and monoclonal antibodies to target specific cells. Given that these nanoparticles are engineered to interact with cells, it is essential to ensure that these modifications do not introduce unintended adverse effects. A critical concern is the physiological responses elicited by degraded nanoparticles and whether bare or coated nanoparticles will biodegrade in the cellular environment.⁴⁵ The MTT results

suggest that Ag-doped Co_3O_4 nanoparticles are more likely to induce cell death compared to pure Co_3O_4 . Consequently, the synthesis of Ag-doped Co_3O_4 nanoparticles, facilitated by *Clerodendrum infortunatum* leaf extract, indicates that these nanoparticles may possess chemotherapeutic properties, which could be explored for the development of novel pharmaceuticals.

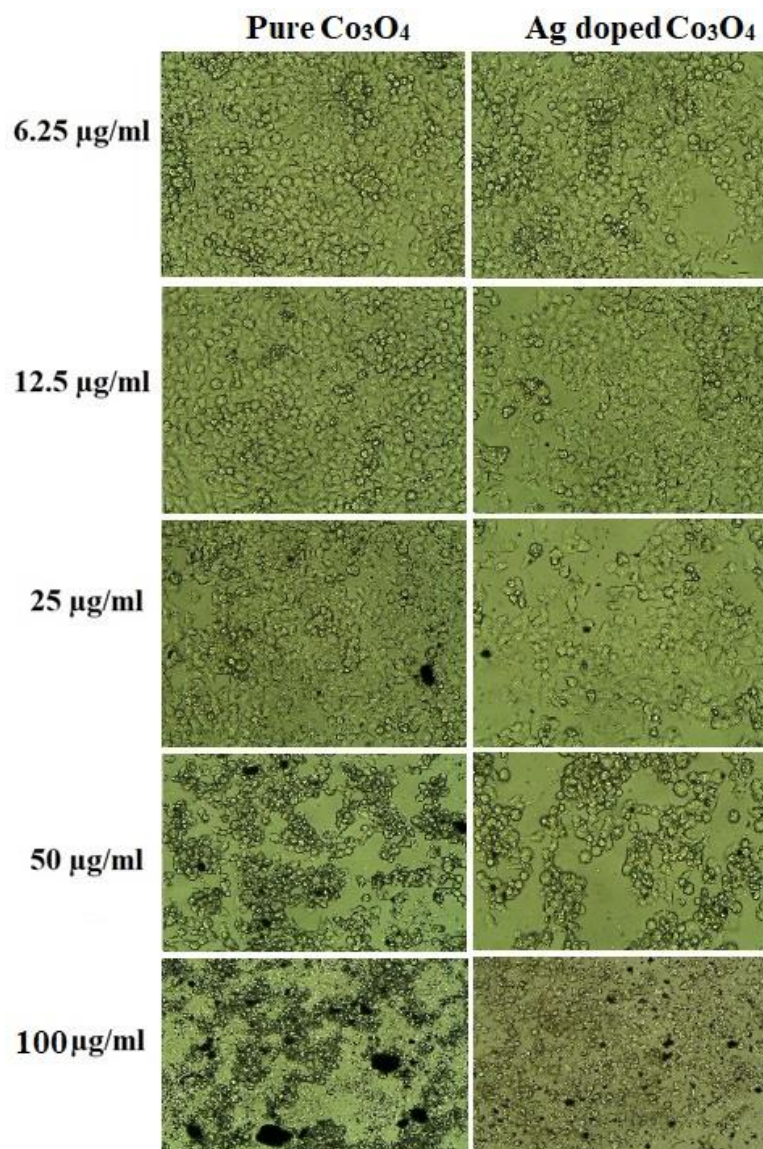


Fig. 9 – Cell numbers and viability evaluated using MTT staining after 24 h seeding. (6.25µg/mL, 12.5µg/mL, 25µg/mL, 50µg/mL and 100µg/mL).

CONCLUSION

In summary, pure and Ag-doped Co_3O_4 nanoparticles synthesized via *Clerodendrum infortunatum* leaf extract exhibited a cubic spinel structure with crystallite sizes of 24.3 nm (pure) and 19.6 nm (doped), spherical morphology (~20 nm), and elemental compositions confirmed by EDS and

XPS (Ag \approx 2.2 at%). UV-Vis spectroscopy showed a red-shift from 290 nm to 296 nm and band-gap energies of 2.54 eV (Co_3O_4) and 2.68 eV (Ag-doped). Photoluminescence revealed reduced emission intensity upon Ag doping, indicating increased non-radiative recombination via oxygen vacancies. MTT assays against AGS gastric adenocarcinoma cells demonstrated dose-dependent

cytotoxicity, with Ag-doped Co_3O_4 achieving 98% cell death at $100 \mu\text{g ml}^{-1}$ compared to 88% for pure Co_3O_4 , owing to enhanced ROS generation and Ag^+ ion release. These findings confirm the successful green synthesis of Ag-doped Co_3O_4 nanoparticles with favorable optical and potent anticancer properties, highlighting their potential for therapeutic and biomedical applications.

REFERENCES

- M. Y. A. Mohamed, H. Ferjani, O. E. Ogunjinmi, M. Jalouli and D. C. Onwudiwe, *Inorganica Chimica Acta*, 2024, 569, 122086.
- L. K. Ruddaraju, S. C. Veerla, V. R. M. Kolapalli, P. N. V. K. Pallela, V. S. Padavala and S.V. N. Pammi, *New J. Chem.*, 2021, 45, 15363–15370.
- L. K. Ruddaraju, S. V. N. Pammi, G. S. Guntuku, V. S. Padavala and V. R. M. Kolapalli, *Asian J. Pharm. Sci.*, 2020, 15, 42–59.
- M. S. Akhtar, J. Panwar and Y.-S. Yun, A. C. S. *Sustain. Chem. Eng.*, 2013, 1, 591–602.
- M. Darroudi, M. Hakimi, M. Sarani, R. K. Oskuee, A. K. Zak and L. Gholami, *Ceramics Int.*, 2013, 39, 6917–6921.
- M. Darroudi, Z. Sabouri, R. K. Oskuee, A. K. Zak, H. Kargar and M. H. N. A. Hamid, *Ceramics Int.*, 2014, 40, 4827–4831.
- N. Thovhogi, A. Diallo, A. Gurib-Fakim and M. Maaza, *J. Alloys Comp.*, 2015, 647, 392–396.
- R. Govindasamy, V. Raja, S. Singh, M. Govindarasu, S. Sabura, K. Rekha, V. D. Rajeswari, S. S. Alharthi, M. Vaiyapuri, R. Sudarmani, S. Jesurani, B. Venkidasamy and M. Thiruvengadam, *Molecules*, 2022, 27, 5646.
- R. V. Poonguzhali, E. R. Kumar, C. Srinivas, M. Alshareef, M. M. Aljohani, A. A. Keshk, N. M. E. Metwally and N. Arunadevi, *Sensors and Actuators B: Chemical*, 2023, 377, 133036–133048.
- J. K. Sharma, P. Srivastava, G. Singh, M. S. Akhtar and S. Ameen, *Mater. Sci. Eng. B.*, 2015, 193, 181–188.
- M. Saeed, N. Akram, S. A. Naqvi, M. Usman, M. A. Abbas, M. Adeel and A. Nisar, *Green Proc. Synth.*, 2019, 8, 382–390.
- P. Saravanakumar, M. Muthukumar, R. R. Muthuchudarkodi and P. Ramkumar, *Int. J. Recent Res. Aspects*, 2018, 918–923.
- P. Cheng, F. Dang, Y. Wang, J. Gao, L. Xu, C. Wang, L. Lv, X. Li, B. Zhang and B. Liu, *Sensors and Actuators B: Chemical*, 2021, 328, 129028–129041.
- D. Barreca, D. B. Ekermann, E. Comini, A. Devi, R. A. Fischer, A. Gasparotto, M. Gavagnin, C. Maccato, C. Sada, G. Sberveglieri and E. Tondello, *Sens. Actuators*, 2011, B 160, 79–86.
- X. W. Chen, S. Wang, C. Su, Y. T. Han, C. Zou, M. Zeng, N. T. Hu, Y. J. Su, Z. H. Zhou and Z. Yang, *Sens. Actuator B Chem.*, 2020, 305, 127393.
- C. Stella, N. Soundararajan and K. Ramachandran, *AIP Advances*, 2015, 5, 087104.
- H. Chen, J. Wang, F. Liao, X. Han, C. Xu and Y. Zhang, *Ceramics International*, 2019, 45, 8008–8016.
- A. F. Alema, A. K. Workua, D. W. Ayelea, T. A. Wubieneh, A. Teshager, T. Kndied, B. T. Admasue, M. A. Teshager, A. A. Asege, M. D. Ambaw, M. A. Zeleke, A. K. Shibesh and T. A. Yemata, *Heliyon*, 2023, 9, 13286.
- M. Aadil, S. Zulfiqar and M. F. Warsi, *Ceramics International*, 2021, 47, 9806–9817.
- X. Bai and Z. Yang, *J. Electrochem. Soc.*, 2021, 168, 107508.
- R. Molavi and M. H. Sheikhi, *Mater. Letters*, 2018, 233, 74–77.
- K. Parveen, V. Banse and L. Ledwani, *Am. Institute of Physics*, 2016, 1724, 020048.
- F. Ameen, *Appl. Sci.*, 2022, 12, 1384.
- R. Singh and S. Dutta, *Advanced Powder Technology*, 2017, 29, 211.
- P. S. Vindhya, S. Sandhya and V. T. Kavitha, *Int. J. Hydrogen Energy*, 2025, 103, 766–786.
- S. Kumar, N. Bithel, S. Kumar, Kishan, M. Sen and C. Banerjee, *South African J. Botany*, 2024, 164, 146.
- A. Sudha, A. A. Banu, N. M. I. Alhaji, D. Saravanakumar, S. Sivaranjani and A. Ayeshamariam, *Res. Jr. Agril. Sci.*, 2022, 13, 322–328.
- M. Silambarasan, S. Saravanan and T. Soga, *Int. J. Chem. Tech. Res.*, 2015, 7, 1644–1650.
- S. Shabna, S. C. Jeyakumar, M. R. Joel, S. S. J. Dhas, S. Aswanthappa, R. S. Kumar, A. I. Almansour, A. Aravind, L. M. Jose and C. S. Biju, *J. Sol-gel Sci. Technol.*, 2025, 115, 1116–1134.
- A. Chandraraj, S. C. Sharma, S. C. Peter and N. S. John, *ACS Appl. Energy Mater.*, 2020, 3, 5439–5447.
- H. S. Wasly, M. S. A. El-Sadek and K. M. Batoo, *Mater. Res. Express*, 2019, 6, 55003.
- X. M. Cao, Z. J. Sun and Z. B. Han, *Material Chemistry Frontiers*, 2021, 5, 6969–6977.
- P. S. Vindhya and V. T. Kavitha, *Inorg. Chem. Comm.*, 2023, 150, 110472.
- S. Iqbal, M. Javed, A. Bahadur, M. A. Qamar, M. Ahmad, M. Shoaib, M. Raheel, N. Ahmad, M. B. Akbar and H. Li, *J. Mater. Sci.: Materials in Electronics*, 2020, 31, 8423.
- J. Fangab and Y. Xuan, *RSC Advances*, 2017, 7, 56023.
- A. Pramotheekumar, N. Senthilkumar, K. C. M. Gnana Malar, M. Meena and I. V. Potheher, *J. Mater. Sci.: Materials in Electronics*, 2019, 30, 19043.
- R. Gopalakrishnana and M. Ashokkumar, *J. Mol. Struct.*, 2021, 1244, 131207.
- H. Siddiqui, M. R. Parra, M. M. Malik and F. Z. Haque, *Optical and Quantum Electronics*, 2018, 50, 260.
- T. Jan, J. Iqbal, U. Farooq, A. Gul, R. Abbasi, I. Ahmad and M. Malik, *Ceram. Int.*, 2015, 41, 13074.
- M. Abudayyak, T. A. Gurkaynak and G. Zhan, *Toxicology and Industrial Health*, 2017, 1–9.
- S. Prabhu, T. D. Thangadurai and P. V. Bharathy, *Nano. Biomed. Eng.*, 2021, 394–400.
- M. E. T. Yazdi, M. S. Amiri, S. Akbari, M. Sharifalhosseini, F. Nourbakhsh, M. Mashreghi, M. R. E. Yousefi, M. Abbasi and A. H. Modarres, *Bio. Nano. Sci.*, 2020, 10, 1121–1127.
- M. J. Akhtar, H. A. Alhadlaq, A. Alshamsan, M. A. M. Khan and M. Ahamed, *Scientific Reports*, 2015, 5, 13876.
- M. Ahamed, M. J. Akhtar, M. A. M. Khan and H. A. Alhadlaq, *ACS Omega*, 2022, 7, 7103.
- N. Lewinski, V. Colvin and R. Drezek, *Cytotoxicity of Nanoparticles*, 2008, 4, 26–49.